Energies **2015**, *8*, 5661-5677; doi:10.3390/en8065661

OPEN ACCESS

energies

ISSN 1996-1073

www.mdpi.com/journal/energies

Article

Performance Analysis of a MCFC/MGT Hybrid Power System Bi-Fueled by City Gas and Biogas

Hongyu Huang [1,*], Jun Li [2], Zhaohong He [1], Tao Zeng [2], Noriyuki Kobayashi [2] and Mitsuhiro Kubota [2]

[1] Guangzhou Institute of Energy Conversion, Chinese Academy of Sciences, Guangzhou 510640, China; E-Mail: hezh@ms.giec.ac.cn

[2] Department of Chemical Engineering, Nagoya University, Nagoya, Aichi 464-8603, Japan; E-Mails: junli@energy.gr.jp (J.L.); zengtao@energy.gr.jp (T.Z.); kobayashi758@163.com (N.K.); kubota758@163.com (M.K.)

* Author to whom correspondence should be addressed; E-Mail: huanghy@ms.giec.ac.cn; Tel.: +86-20-3721-0762; Fax: +86-20-8701-3240.

Academic Editor: Haolin Tang

Received: 27 March 2015 / Accepted: 1 June 2015 / Published: 15 June 2015

Abstract: This study evaluates the performance of a molten carbonate fuel cell and micro gas turbine (MCFC/MGT) hybrid power system bi-fueled by city gas and biogas. The performance of the MCFC/MGT hybrid power system and MFCF/MGT hybrid power system response have been investigated experimentally and numerically. Results show that the MCFC, steam reformer, and catalytic combustor models are in agreement with the experimental results of the system fueled by city gas only and the system bi-fueled by city gas and biogas. The MFCF/MGT hybrid power system can have manifest operation with the addition of biogas at a flow rate of up to 150.0 $Nm^3 \cdot h^{-1}$, which is about 50% of the overall input heat value. In addition, the MCFC and MGT outputs decrease with the increase in the flow rate of added biogas, with an overall power generation efficiency ranging from 39.0% to 42.0%. Furthermore, the MCFC/MGT hybrid power system can be operated stably both at low amplitude with slow current change and large amplitude with rapid power conditions. Finally, the MCFC/MGT hybrid system bi-fueled by city gas and biogas may be applicable to the energy supply of the micro–grid network.

Keywords: biogas and city gas; bi-fueled; molten carbonate fuel cell; micro gas turbine; hybrid system; micro-grid network

1. Introduction

With the steadily increasing oil prices and strict policies for emission control, the development of new, high efficiency power generation concepts has become increasingly urgent in recent decades. The molten carbonate fuel cell (MCFC) has attracted great interest because it is a promising, clean, and efficient technology for high-efficiency and low-emission power production [1–3]. MCFCs operate under high temperature conditions, and thus, can cogenerate power with different generators, such as humid air turbines (HATs) or gas turbines (GTs) [4–7].

The outlet gas from a fuel cell contains high–temperature thermal energy and unreacted fuel. Thus, this gas can be used as combustor fuel and heat source of a steam reformer to improve the energy efficiency of the MCFC system [7]. Burning the outlet gas via a conventional combustor is difficult owing to its flammability limits, hence the application of catalytic combustion, a chemical process that efficiently burns fuel in concentrations outside the flammability limit and reduces the formation of undesired by-products, such as unburned hydrocarbons (UHCs), CO and NO_x [8–12]. Catalytic combustion has low emissions and has been used in different applications, including MCFCs [13–15].

MCFC/MGT hybrid systems have been developed in different fields is promising, high–efficiency, and low-emission systems [16–18]. Wee [16] studied the MCFC/GT cogeneration performance in indirect and direct MCFC/GT hybrid systems, and found that the indirect system is more suitable for relatively small-scale systems with micro GT than the direct system. Liu [17] designed a hybrid power system that includes a pressurized MCFC with MGT using the turbine inlet and cell operating temperatures near the design value for best efficiency. However, the high pressure loss between the compressor and the turbine hindered the gas turbine from attaining the original power. Lunghi [18] evaluated the effect of the fuel utilization coefficient and fuel cell section size on high-modulus carbon fiber (HMCF) cell heated gas turbines, and found that a cell optimized for stand-alone operations is not necessarily optimized for integration in a hybrid cycle. Moreover, the efficiency cannot go higher than 58% without new gas turbine designs.

Biogas is a gas rich in CH_4 and CO_2. It is derived from animal waste, human sewage, or biomass, and is an environmentally friendly and practical alternative fuel [19–22]. Kivisaari [19] evaluated MCFCs by deploying a biomass-fueled integrated gasification combined cycle (IGCC) system in which biomass was converted into biogas by pressurized gasification with subsequent treatment. The results showed that the IGCC-MCFC systems fueled by biomass have a maximum efficiency of 43%. Hamad *et al*. [20] investigated the performance of a combined heat, hydrogen and power system (CHHP) for the Missouri University of Science and Technology campus fed by biogas from anaerobic digestion, and they found that the CHHP system could provide approximately 22,000 kW h and 650 kg of hydrogen to the university campus per day, therefore, the MCFC fuel cell system fed by biogas was able to reduce fossil fuel usage and greenhouse gas emissions. Milewski [21] developed a reduced order model for modeling the effect of fuel and oxidant flows on MCFC performance. As the inlet fuel was rich in H_2 (and CO_2),

the fuel composition varied over the cell surface and throughout the stack. The results showed that the proposed model was very light and serviceable for system level performance prediction. Bove [22] experimentally investigated the MCFC performance using three different biogas types and methane, and reported that all biogas types exhibited high potential for use as MCFC system fuels.

The above research shows that very little research has been conducted on the effect of the MCFC/MGT hybrid system on the energy supply in a micro–grid network, hence it is necessary to develop a MCFC/MGT hybrid system model and investigate the possibility of using different fuels on this hybrid system to supply energy to the power grid network. This study therefore develops a MCFC/MGT hybrid system model and investigates the operating performance of a MCFC/MGT hybrid power system bi-fueled by city gas and biogas. The research objectives are as follows: first, to develop the MCFC, steam reformer, and catalytic combustor models; second, to evaluate the performance of a MCFC/MGT hybrid power system when bi-fueled by city gas and biogas; and third, to study the possibility of using an MCFC/MGT hybrid system fueled by bi-fueled of city gas and biogas to supply energy to the power grid network. Experiments and simulations are used to examine the performance during the operation of the hybrid system for the MCFC/MGT power generation, steam reformer, and catalytic combustor systems. Response analyses of the MCFC system are also considered in this study for the MCFC power generation and supply system.

2. Numerical Modeling and Experimental System

The model units of the MCFC/MGT hybrid system used in this research consisted of a MCFC and MGT for power generation, a steam reformer for producing CO and H_2 (the MCFC inlet fuel), and a catalytic combustor for supplying heat to the steam reformer. The development of the MCFC, steam reformer, and catalytic combustor models are discussed in the following sections.

2.1. Molten Carbonate Fuel Cell Model

The MCFC model in this study was based on co-flow planar 170 kW level MCFC stack module with 250 cells and Li_2CO_3 electrolyte. The schematic diagram of one cell stack is shown in Figure 1.

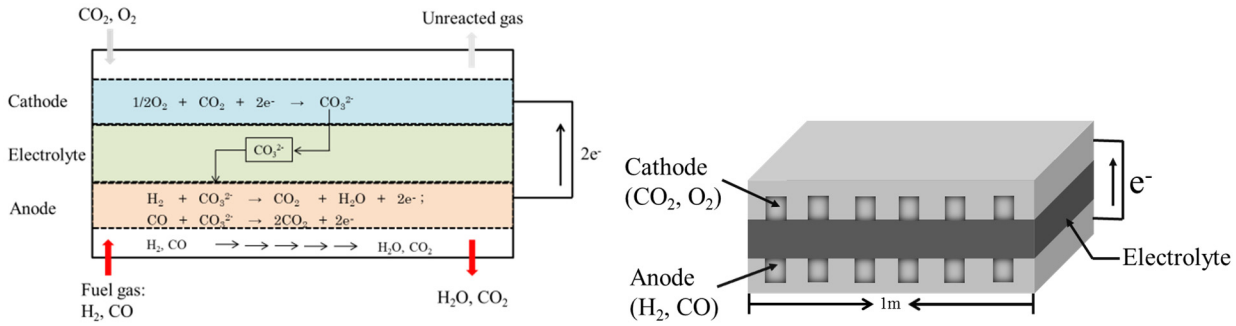

Figure 1. Molten carbonate fuel cell model.

The following conditions were assumed to simplify the modeling:

(1) The cells in the module are similar to each other;
(2) The boundaries for each cell are adiabatic;
(3) The anode, cathode, and electrolyte layers are considered as one layer during thermal analysis.

The MCFC model consists of both the electrochemical and thermal models. In a cell stack, the input gas temperature was approximately 580 °C and the output temperature was 670 °C, with a 100 °C temperature slip. The cell stack was cut into 200 cells in this model. Power was generated through the following electrochemical reactions [22–25]:

$$\text{Anode: } H_2 + CO_3^{2-} \rightarrow CO_2 + H_2O + 2e^- \quad (1)$$

$$CO + CO_3^{2-} \rightarrow 2CO_2 + 2e^- \quad (2)$$

$$\text{Cathode: } 1/2\,O_2 + CO_2 + 2e^- \rightarrow CO_3^{2-} \quad (3)$$

$$\text{Overall reactions: } H_2 + 1/2\,O_2 \rightarrow H_2O + 2e^- + 241.8\ \text{kJ} \cdot \text{mol}^{-1} \quad (4)$$

$$CO + 1/2\,O_2 \rightarrow CO_2 + 2e^- + 41.1\ \text{kJ} \cdot \text{mol}^{-1} \quad (5)$$

The cell current was determined by the electronic flow through the electrochemical reaction and expressed as Faraday's law:

$$n(e^-) = i/2F \quad (6)$$

where $n(e^-)$ is the mole flow of electrons (kmol·h^{-1}); i is current value (A); F is the Faraday constant (h·A·kmol^{-1}).

The operating voltage, which is related to the composition of fuel and oxide gas, partial pressure, temperature, and current value, is written as follows:

$$V \cong E - (R_{\text{ir}} + R_{\text{a}} + R_{\text{c}}) \times j \quad (7)$$

where j is current density, E is Nernst voltage, which is the function of standard electrode potential (E^0), temperature (T) and gas partial pressure (P) in the anode and cathode as shown in Equation (3).

$$E = E^0 + \frac{RT}{2F} \ln \frac{P_{\text{H}_2\text{a}} \cdot P_{\text{CO}_2\text{c}} \cdot {P_{\text{O}_2\text{c}}}^{1/2}}{P_{\text{CO}_2\text{a}} \cdot P_{\text{H}_2\text{Oc}}} \quad (8)$$

Anode and cathode resistance depends on the materials comprising the nodes, as well as the internal resistance on the electrolyte, which can be calculated as follows:

$$R_{\text{ir}} = A_{\text{ir}} \cdot \exp\left(-\frac{\Delta H_{\text{ir}}}{R \cdot T}\right) \quad (9)$$

$$R_{\text{a}} = A_{\text{a}} \cdot T \cdot \exp\left(-\frac{\Delta H_{\text{a}}}{R \cdot T}\right) \quad (10)$$

$$R_{\text{c}} = A_{\text{c1}} \cdot T \cdot \exp\left(-\frac{\Delta H_{\text{c1}}}{R \cdot T}\right) P_{\text{O}_2}^{-0.75} \cdot P_{\text{CO}_2}^{0.5} + A_{\text{c2}} \cdot T \cdot \exp\left(-\frac{\Delta H_{\text{c2}}}{R \cdot T}\right) \left\{m_{\text{CO}_2} + A_{\text{c3}} \cdot m_{\text{H}_2\text{O}} \cdot \exp\left(-\frac{\Delta H_{\text{c3}}}{R \cdot T}\right)\right\}^{-1} \quad (11)$$

where A is the frequency factor, and ΔH is the activation energy. Table 1 lists the values of each frequency factors and activation energy [23,25].

Table 1. Frequency factor and activation energy values.

Items	Value	Unit
A_{ir}	9.84×10^{-3}	ohm·cm^2
ΔH_{ir}	23.80	kJ·mol^{-1}
A_{a}	9.50×10^{-7}	ohm·cm^2·atm$^{0.5}$·K^{-1}
ΔH_{a}	27.90	kJ·mol^{-1}
A_{c1}	6.91×10^{-15}	ohm·cm^2·atm$^{0.5}$·K^{-1}
ΔH_{c1}	179.20	kJ·mol^{-1}
A_{c2}	3.75×10^{-9}	ohm·cm^2·K^{-1}
ΔH_{c2}	67.10	kJ·mol^{-1}
A_{c3}	1.07×10^{-6}	ohm·cm^2
ΔH_{c3}	95.20	kJ·mol^{-1}

The power of the MCFC (P) was obtained by current (I) and voltage (V), as shown in Equation (12):

$$P = I \cdot V \tag{12}$$

The electrolyte may determine fuel consumption in mass balance. In this model, the mass balance of each species was considered, along with detailed thermal conductivity and transport properties such as density, specific heat capacity, thermal conductivity and dynamic viscosity.

Mass balance of anode channel:

$$F_{\mathrm{outlet}}[\mathrm{H_2}] = F_{\mathrm{inlet}}[\mathrm{H_2}] + r[\mathrm{H_2}] \tag{13}$$

$$F_{\mathrm{outlet}}[\mathrm{CO}] = F_{\mathrm{inlet}}[\mathrm{CO}] - r[\mathrm{CO}] \tag{14}$$

$$F_{\mathrm{outlet}}[\mathrm{H_2O}] = F_{\mathrm{inlet}}[\mathrm{H_2O}] + r[\mathrm{H_2O}] \tag{15}$$

$$F_{\mathrm{outlet}}[\mathrm{CO_2}] = F_{\mathrm{inlet}}[\mathrm{CO_2}] + r[\mathrm{CO_2}] \tag{16}$$

Mass balance of cathode channel:

$$F_{\mathrm{outlet}}[\mathrm{CO_2}] = F_{\mathrm{inlet}}[\mathrm{CO_2}] - 1/2\, n(\mathrm{e^-}) \tag{17}$$

$$F_{\mathrm{outlet}}[\mathrm{O_2}] = F_{\mathrm{inlet}}[\mathrm{O_2}] - 1/4\, n(\mathrm{e^-}) \tag{18}$$

where F_{inlet} is the inlet flow rate of chemicals (kmol·h^{-1}), $\mathrm{F_{outlet}}$ is the inlet flow rate of chemicals (kmol·h^{-1}), and r is reaction rate of chemicals (kmol·h^{-1}).

The energy balance included heat transfer and energy change, which also involved the electrical power and the enthalpy changes of the chemical and electrochemical reactions. Gas temperature was calculated from enthalpy, which depends on the square of the temperature. Energy balance equations are shown in Equations (19)–(22). The parameter values of a, b, and c used in Equation (22) are listed in Table 2 [25,26]:

$$Q_{\mathrm{outlet}} = Q_{\mathrm{inlet}} + Q_{\mathrm{generation}} - Q_{\mathrm{power}} \tag{19}$$

$$Q_{\mathrm{generation}} = 1/2\, n(\mathrm{e^-}) \times 241.8 + r[\mathrm{CO}] \times 41.1 \tag{20}$$

$$Q_{\mathrm{power}} = P \tag{21}$$

$$Q_{\mathrm{outlet}} = \sum H = a + bT_{\mathrm{outlet}} + cT_{\mathrm{outlet}}^2 \tag{22}$$

Table 2. Parameter values of enthalpy on temperature.

Species	*a*	*b*	*c*
CH_4	−8.73653	0.025966	2.20×10^{-5}
C_2H_6	−9.12764	0.016874	6.06×10^{-5}
C_3H_8	−12.5028	0.0209687	9.08×10^{-5}
C_4H_{10}	−17.1319	0.0308405	1.17×10^{-4}
H_2	−7.65941	0.0276503	1.43×10^{-6}
CO	−7.68459	0.0273887	2.73×10^{-6}
H_2O	−8.77673	0.0309842	4.20×10^{-6}
CO_2	−10.7092	0.0370774	7.79×10^{-6}
O_2	−8.00066	0.0284986	2.90×10^{-6}
N_2	−7.6341	0.0272345	2.61×10^{-6}

Heat transfer between the MCFC and the anode/cathode is shown in Equations (23)–(25):

$$Q_{\text{tran}} = h \times A \times \left(T_{\text{gas}} - T_{\text{MCFC}}\right) \tag{23}$$

$$h = Nu \times k/D \tag{24}$$

$$Nu = 0.664 \times Pr^{1/3} \times Re^{1/2} \tag{25}$$

$$U_{\text{f}} = (Q_{\text{inlet}}[\text{H}_2][\text{CO}] - Q_{\text{outlet}}[\text{H}_2][\text{CO}])/(Q_{\text{inlet}}[\text{H}_2][\text{CO}]) \tag{26}$$

The fuel consumption ratio was calculated to evaluate the performance of MCFC in Equation (26). The set of equations describing the model was implemented in Visual Modeler software to simulate the MCFC performance.

2.2. Steam Reformer Model

The reforming fuel used in this study was tower gas, which includes methane, ethane, propane, and butane. Fuel steam reforming involves following five reactions: reforming reactions as shown in Equations (27)–(30), and the water–gas–shift reaction as shown in Equation (31). Reforming reactions are endothermic, whereas the water–gas–shift reaction is exothermic. The reaction scheme in the steam reformer model is as follows [22–25]:

Reforming reactions:

$$\text{CH}_4 + \text{H}_2\text{O} \rightarrow \text{CO} + 3\text{H}_2, \qquad \Delta H_{298}^0 = 206.1\ \text{kJ} \cdot \text{mol}^{-1} \tag{27}$$

$$\text{C}_2\text{H}_6 + 2\text{H}_2\text{O} \rightarrow 2\text{CO} + 5\text{H}_2, \qquad \Delta H_{298}^0 = 347.0\ \text{kJ} \cdot \text{mol}^{-1} \tag{28}$$

$$\text{C}_3\text{H}_8 + 3\text{H}_2\text{O} \rightarrow 3\text{CO} + 7\text{H}_2, \qquad \Delta H_{298}^0 = 498.6\ \text{kJ} \cdot \text{mol}^{-1} \tag{29}$$

$$\text{C}_4\text{H}_{10} + 4\text{H}_2\text{O} \rightarrow 4\text{CO} + 9\text{H}_2, \qquad \Delta H_{298}^0 = 650.2\ \text{kJ} \cdot \text{mol}^{-1} \tag{30}$$

Water gas shift reaction:

$$\text{CO} + \text{H}_2\text{O} \rightarrow \text{CO}_2 + \text{H}_2, \qquad \Delta H_{298}^0 = -41.4\ \text{kJ} \cdot \text{mol}^{-1} \tag{31}$$

The reformer reactor model is shown in Figure 2, and the mass balance equations for all species are shown in Equations (32)–(39).

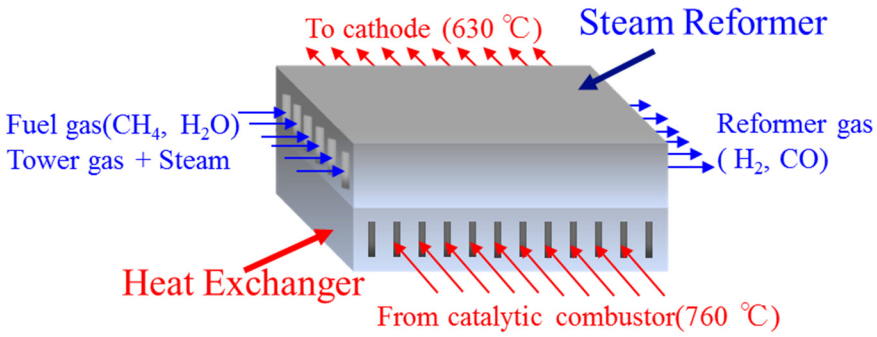

Figure 2. Fuel steam reformer model.

$$F_{\text{outlet}}[\text{CH}_4] = F_{\text{inlet}}[\text{CH}_4] - r[\text{CH}_4] \quad (32)$$

$$F_{\text{outlet}}[\text{C}_2\text{H}_6] = F_{\text{inlet}}[\text{C}_2\text{H}_6] - r[\text{C}_2\text{H}_6] \quad (33)$$

$$F_{\text{outlet}}[\text{C}_3\text{H}_8] = F_{\text{inlet}}[\text{C}_3\text{H}_8] - r[\text{C}_3\text{H}_8] \quad (34)$$

$$F_{\text{outlet}}[\text{C}_4\text{H}_{10}] = F_{\text{inlet}}[\text{C}_4\text{H}_{10}] - r[\text{C}_4\text{H}_{10}] \quad (35)$$

$$F_{\text{outlet}}[\text{H}_2\text{O}] = F_{\text{inlet}}[\text{H}_2\text{O}] - r[\text{CO}] - r[\text{CH}_4] - 2r[\text{C}_2\text{H}_6] - 3r[\text{C}_3\text{H}_8] - 4r[\text{C}_4\text{H}_{10}] \quad (36)$$

$$F_{\text{outlet}}[\text{CO}] = F_{\text{inlet}}[\text{CO}] + r[\text{CO}] + 2r[\text{C}_2\text{H}_6] + 3r[\text{C}_3\text{H}_8] + 4r[\text{C}_4\text{H}_{10}] \quad (37)$$

$$F_{\text{outlet}}[\text{H}_2] = F_{\text{inlet}}[\text{H}_2] + r[\text{CO}] + 3r[\text{CH}_4] + 5r[\text{C}_2\text{H}_6] + 7r[\text{C}_3\text{H}_8] + 9r[\text{C}_4\text{H}_{10}] \quad (38)$$

$$F_{\text{outlet}}[\text{CO}_2] = F_{\text{inlet}}[\text{CO}_2] + r[\text{CO}] \quad (39)$$

The reaction rates of the fuels are shown in Equations (40)–(43):

$$r[\text{CH}_4] = k_1 \times cat_{\text{w}} \times \frac{P[\text{CH}_4]}{101.3} \times \left\{ \frac{101.3}{1 + k_2 \times \frac{P[\text{H}_2\text{O}]}{P[\text{H}_2]} + k_3 \times \frac{P[\text{CO}]}{101.3}} \right\}^7 \quad (40)$$

where cat_{w} is the weight of catalyst ($\text{kg}_{\text{catlyst}}$), $k_1 = 4.37 \times 10^8 \times \exp\left(\frac{-1.88\times10^5}{g_c T}\right)$, $k_2 = 2.27 \times \exp\left(\frac{-3.94\times10^5}{g_c T}\right)$, and $k_3 = 4.37 \times 10^{-15} \times \exp\left(\frac{2.75\times10^5}{g_c T}\right)$.

$$r[\text{C}_2\text{H}_6] = 1.503 \times cat_{\text{w}} \times \exp\left(\frac{-18100}{4.184 \times g_c T}\right) \times \left(\frac{P[\text{C}_2\text{H}_6]}{101.3}\right)^{0.54} \times \left(\frac{P[\text{H}_2\text{O}]}{101.3}\right)^{-0.33} \times \left(\frac{P[\text{H}_2]}{101.3}\right)^{0.2} \quad (41)$$

$$r[\text{C}_3\text{H}_8] = 1.503 \times cat_{\text{w}} \times \exp\left(\frac{-21000}{4.184 \times g_c T}\right) \times \left(\frac{P[\text{C}_3\text{H}_8]}{101.3}\right)^{0.8} \times \left(\frac{P[\text{H}_2\text{O}]}{101.3}\right)^{-0.45} \quad (42)$$

$$r[\text{C}_4\text{H}_{10}] = 1.503 \times cat_{\text{w}} \times \exp\left(\frac{-24000}{4.184 \times g_c T}\right) \times \left(\frac{P[\text{C}_4\text{H}_{10}]}{101.3}\right)^{1} \times \left(\frac{P[\text{H}_2\text{O}]}{101.3}\right)^{-0.6} \quad (43)$$

The energy balance in the reformer is given by Equations (44)–(46):

$$Q_{\text{outlet}} = Q_{\text{inlet}} - Q_{\text{ref}} + Q_{\text{he}} \quad (44)$$

where Q_{ref} the reformer reaction expressed as follows:

$$Q_{\text{ref}} = 201.6 \times r[\text{CH}_4] + 347.0 \times r[\text{C}_2\text{H}_6] + 498.6 \times r[\text{C}_3\text{H}_8] + 650.2 \times r[\text{C}_4\text{H}_{10}] - 41.1 \times r[\text{CO}] \quad (45)$$

Q_{he} is the amount of heat exchange, as shown in Equation (46):

$$Q_{he} = U \times (T_h - T_f) \quad (46)$$

Temperature is dependent on the change in enthalpy, as described in the MCFC model. The set of equations describing the model was implemented in Visual Modeler software to simulate the steam reformer performance.

2.3. Catalytic Combustor Model

The catalytic combustor model is shown in Figure 3. The fuel was obtained from the unreacted anode gas, and the air was from MGT. Combustion heat was used to carry out the steam reformer reaction. The reaction scheme in the catalytic combustor model is as follows [22–25]:

$$CH_4 + 2O_2 \rightarrow 2H_2O + CO_2, \quad \Delta H^0_{298} = -802.3\ \text{kJ} \cdot \text{mol}^{-1} \quad (47)$$

$$C_2H_6 + 7/2\ O_2 \rightarrow 3H_2O + 2CO_2, \quad \Delta H^0_{298} = -1428.0\ \text{kJ} \cdot \text{mol}^{-1} \quad (48)$$

$$C_3H_8 + 5O_2 \rightarrow 4H_2O + 3CO_2, \quad \Delta H^0_{298} = -2043.0\ \text{kJ} \cdot \text{mol}^{-1} \quad (49)$$

$$C_4H_{10} + 13/2\ O_2 \rightarrow 5H_2O + 4CO_2, \quad \Delta H^0_{298} = -2658.0\ \text{kJ} \cdot \text{mol}^{-1} \quad (50)$$

$$H_2 + 1/2\ O_2 \rightarrow H_2O, \quad \Delta H^0_{298} = -241.8\ \text{kJ} \cdot \text{mol}^{-1} \quad (51)$$

$$CO + 1/2\ O_2 \rightarrow CO_2, \quad \Delta H^0_{298} = -283.0\ \text{kJ} \cdot \text{mol}^{-1} \quad (52)$$

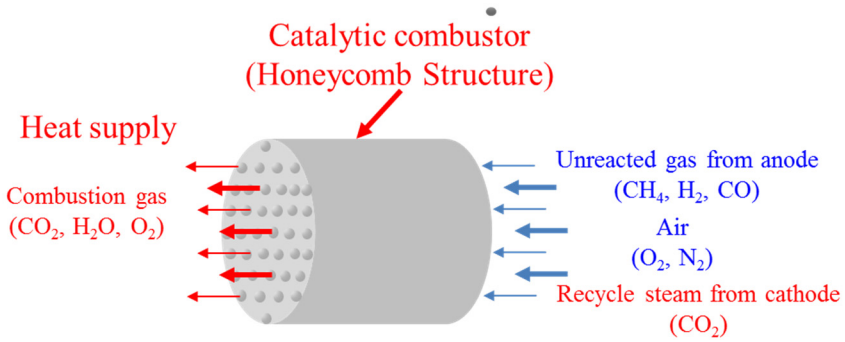

Figure 3. Catalytic combustor model.

In the catalytic combustor model, the fuel was completely consumed and transformed to CO_2 and H_2O. The energy balance is shown in Equations (53) and (54):

$$Q_{outlet} = Q_{inlet} + Q_{reaction} \quad (53)$$

where $Q_{reaction}$ is the heat released from combustion reaction and expressed as follow:

$$Q_{reaction} = 802.3 \times F[CH_4] + 1428.0 \times F[C_2H_6] + 2043.0 \times F[C_3H_8] + 2658.0 \times F[C_4H_{10}] + 241.8 \times F[H_2] + 283.0 \times F[CO] \quad (54)$$

The temperature is dependent on the change in enthalpy, as described in the MCFC model and catalytic reformer model. The set of equations describing the model was implemented in Visual Modeler software to simulate the catalytic combustion performance.

2.4. Experimental System

The experimental test on MCFC/MGT hybrid system used in this work is shown schematically in Figure 4. There are two stacks in the MCFC with 140 cells and an electrode area of 1.015 m^2 for each stack. Only the inlet and outlet temperatures of the cathode and anode with MCFC power can be measured because the MCFC was set in a high pressure vessel. A MGT (TPC50RA, Toyota Turbine & Systems, Toyota, Japan) have been used to cogenerate by using the exhaust gas from the MCFC. The MGT is a single-shaft gas turbine with high speed and direct drive alternator. The maximum rotation speed of MGT is 80,000 rpm. The performance details of the MCFC/MGT hybrid system are listed in Table 3. The MCFC/MGT hybrid system uses city gas as its fuel. A maximum efficiency of 52% at 300 kW was obtained when this fuel was used.

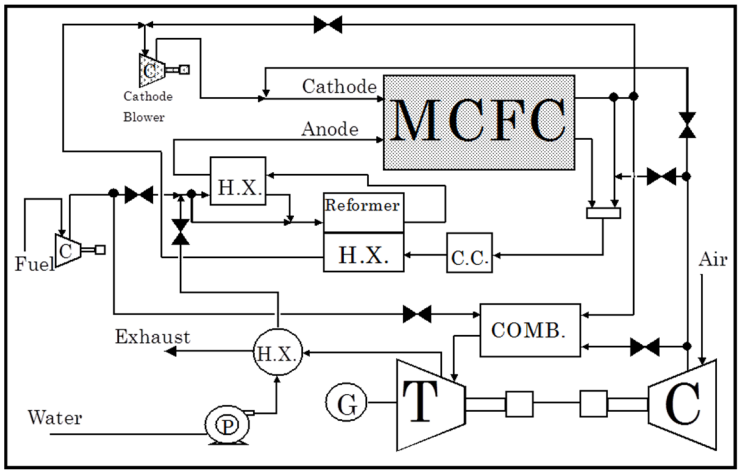

Figure 4. Schematic diagram of the MCFC/MGT hybrid system (Note: H.X.: Heat exchanger; C: Compressor; P: Water Pump; C.C.: Catalytic combustor; T: micro gas turbine; COMB.: Assistance combustor).

Table 3. MCFC/MGT hybrid system performance.

MCFC Stack	2 Stacks
Operation pressure (MPa)	0.335
Cell Voltage (V)	0.726
Current Density (mA·cm^2)	158
Stack temperature (°C)	580/670
MCFC power (kW)	300
MGT power (kW)	50

3. Results and Discussion

3.1. Model Verification

Figure 5 shows the comparison of experimental and calculated values of MCFC and MGT fueled by city gas only at the outset. In the experiment, the output power of MCFC was increased from 170 kW to 230 kW in increments of 5 kW·min^{-1}. The current value and MGT power were obtained at a certain output power which is shown as a dot in Figure 5. A solid line represents the calculated value. The power

of both MCFC and MGT increased with increasing current. Moreover, the experimental and calculated values of MCFC and MGT power with current showed good agreement. Thus the current model is acceptable for analyzing the performance of the MCFC/MGT hybrid power system.

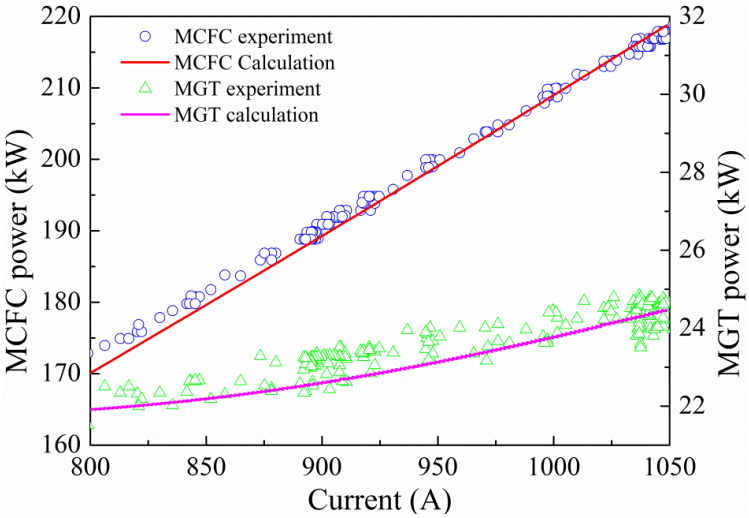

Figure 5. Comparison of experimental and modeling values.

City gas and biogas were used as the two fuels for the MCFC/MGT system in this study. The properties of these fuels are shown in Table 4. Considering that the heat value of biogas is only about one-tenth that of city gas, the applicability of the model needs to be studied using biogas as a bi-fuel for MCFC. Table 5 shows the comparison of the calculated and experimental results of the MCFC and MGT power, cathode inlet, and outlet temperature when 10 and 20 $Nm^3 \cdot h^{-1}$ biogas is added as MCFC fuel. The MCFC/MGT system was started at a standard output of 170 kW, after which the biogas was added to the fuel supply system. Table 5 shows that the differences between calculated and experimental results are all less than 5%, indicating good agreement between calculated and experimental results. From the aforementioned discussion, we can conclude that the current model is suitable for analyzing the performance of MCFC/MGT hybrid power system bi-fuel by city gas and biogas.

Table 4. Properties of city gas and biogas.

City Gas (13A)			Biogas		
Species	**Fraction (%)**	**Heat Value ($kJ \cdot mol^{-1}$)**	**Species**	**Fraction (%)**	**Heat Value ($kJ \cdot mol^{-1}$)**
CH_4	88.0	802.3	CH_4	0.5	802.3
C_2H_6	6.0	1428	N_2	48.2	-
C_3H_8	4.0	2043	CO_2	17.8	-
C_4H_{10}	2.0	2658	CO	21.6	283.0
-	-	-	H_2	11.9	241.8
Sum	100.0	926.8	-	100.0	93.9

Table 5. Performance of MCFC with output of 170 kW after adding 10 and 20 $Nm^3 \cdot h^{-1}$ of biogas with city gas.

Biogas Flow	Items	Power		Cathode Temperature	
		MCFC	MGT	Inlet	Outlet
$Nm^3 \cdot h^{-1}$		kW	kW	°C	°C
10	Experiment	148.4	21.66	579.9	629
	Calculation	146.3	21.6	578	626
	Difference (%)	1.5	0.4	0.3	0.48
20	Experiment	148.3	21.5	580.1	638.6
	Calculation	147.5	21.8	578.1	628.1
	Difference (%)	0.5	1.3	3.5	1.6

3.2. Effect of City Gas and Biogas Bi-Fuel

Figures 6 and 7 show the effect of the added biogas flow rate on the MCFC output, MCFC+MGT output, and power generation efficiency. The MCFC/MGT system started at a standard output of 170 kW fueled by city gas only, then the added biogas flow rate was increased from 10 to 150 $Nm^3 \cdot h^{-1}$ in increments of 10 $Nm^3 \cdot h^{-1}$ with the same overall input heat value of 1210 kW. Figure 6 shows that the MCFC/MGT hybrid power system can be stably operated at a maximum biogas flow of 150 $Nm^3 \cdot h^{-1}$, or approximately 50% of the overall input heat value. Furthermore, the MCFC output decreased with increasing flow rate of the added biogas, and the output of the MCFC/MGT system decreased noticeably when the flow rate of added biogas increased more than 150 $Nm^3 \cdot h^{-1}$. The MCFC+MGT output and power generation efficiency also decreased with increased flow rate of added biogas because the inlet heat value of MCFC (CO and H_2 from outlet of steam reformer) decreased with the increasing flow rate of added biogas, as shown in Figure 8. However, the MCFC/MGT hybrid power system operates stably with a high overall power generation efficiency higher than 39.0%. Based on simulation, the MCFC/MGT hybrid system bi-fueled by city gas and biogas can be applied to supply energy to the micro-grid network.

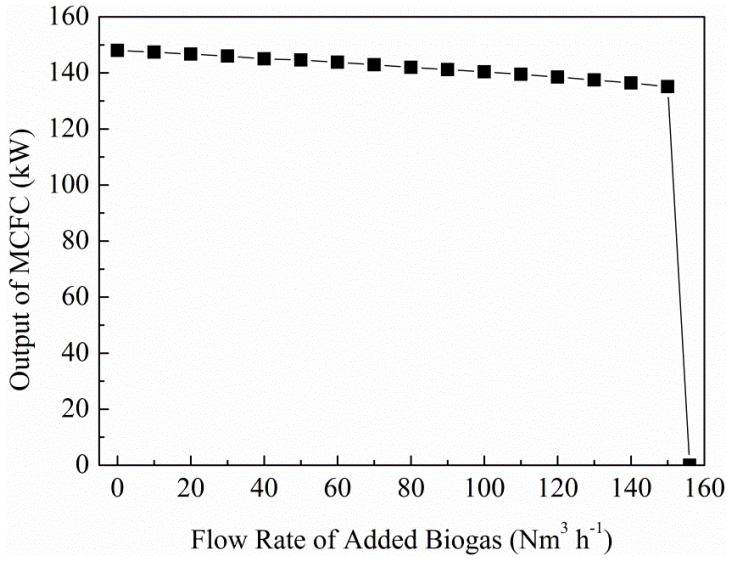

Figure 6. Effect of flow rate of added biogas on output of MCFC.

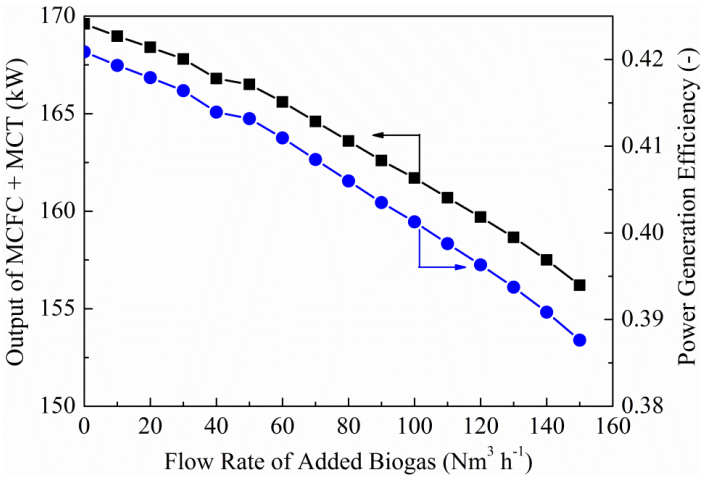

Figure 7. Effect of flow rate of added biogas on output of MCFC+MGT and power generation efficiency.

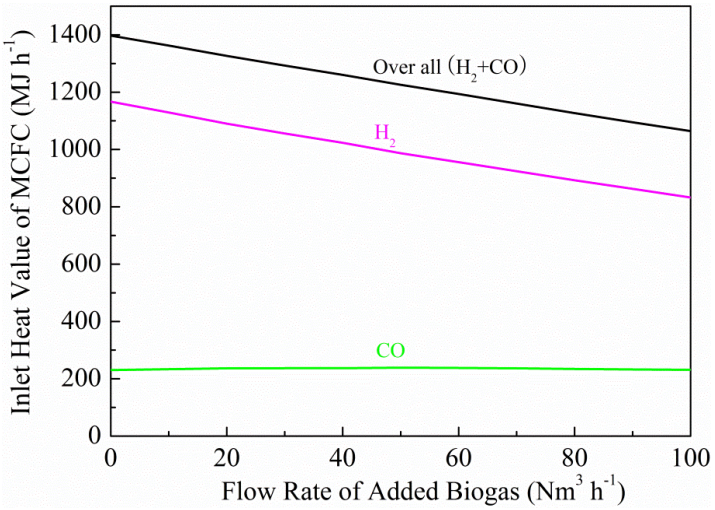

Figure 8. Effect of flow rate of added biogas on inlet heat value of MCFC.

Figure 9 shows the changes in fuel gas composition with the addition of biogas. The concentration of methane in the fuel gas decreased with the increasing flow rate of biogas in the fuel, leading to a drop in H_2 concentration in the outlet of steam reformer, as shown in Figure 10. The CO and CH_4 concentrations in the outlet of the steam reformer remained nearly unchanged, even with the increase of biogas in the fuel. The changes in the outlet of steam reformer gas induce the inlet heat value of MCFC to decrease with the increasing flow rate of added biogas, as shown in Figure 8.

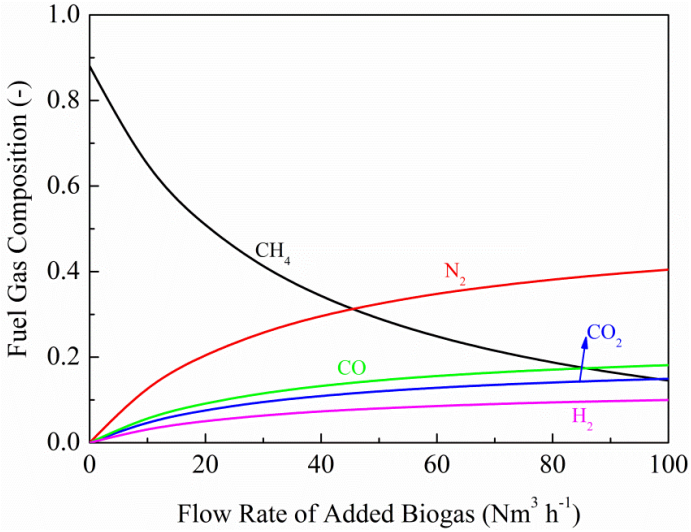

Figure 9. Effect of flow rate of added biogas on fuel gas composition.

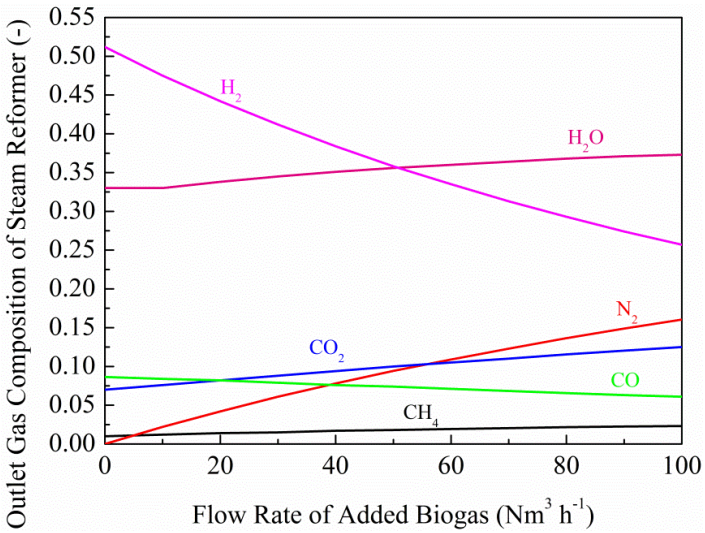

Figure 10. Effect of flow rate of added biogas on outlet gas composition of steam reformer.

3.3. System Response Analysis

In the power supply system, the demanded current, namely alternating current and a sine function of time, and the power change with time. The importance given to MCFC/MGT system response is evident in the conduct of system response analysis at different demanded currents and powers. The MCFC/MGT system starts at a standard output of 170 kW. The demanded current is changed with low amplitudes of 5%, 10%, 15% and 20% as well as with a slow change speed of $\pi/180$ (rad·s^{-1}). Figure 11 shows the function of MCFC and MGT power with time at different demanded currents ranging from 5% to 20%. The demanded power and MCFC output power can be supplied stably over time, *i.e.*, the system can be supplied with the demanded current and power for different current change demands.

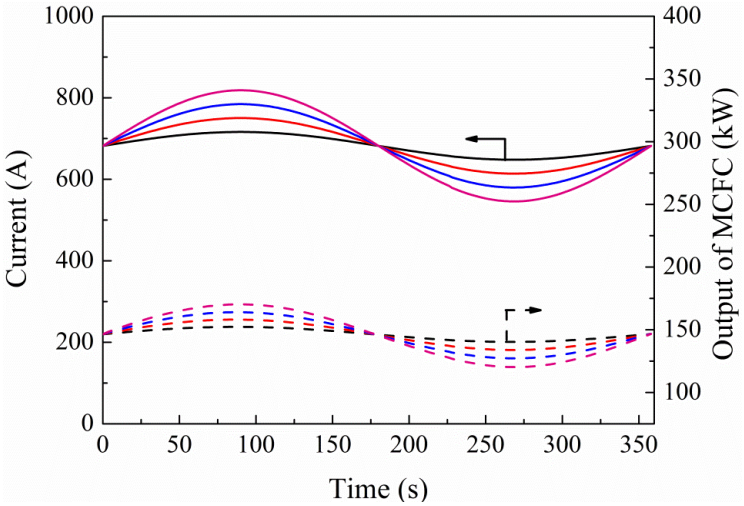

Figure 11. Output response of current (solid line) and output of MCFC (dashed line) at varied power demand changes of 5% (black), 10% (red), 15% (blue), and 20% (pink) at current change speed of π/180.

Figure 12 shows the function of MCFC and MGT power with time at different demanded currents changed with large amplitudes of 5%, 20%, and 40% as well as with a rapid change speed of $\pi/2$ (rad·s^{-1}). Power and current can be also supplied stably with time at larger amplitude and rapid change speed conditions. Therefore, the MCFC/MGT hybrid power system can be operated stably at different demand currents.

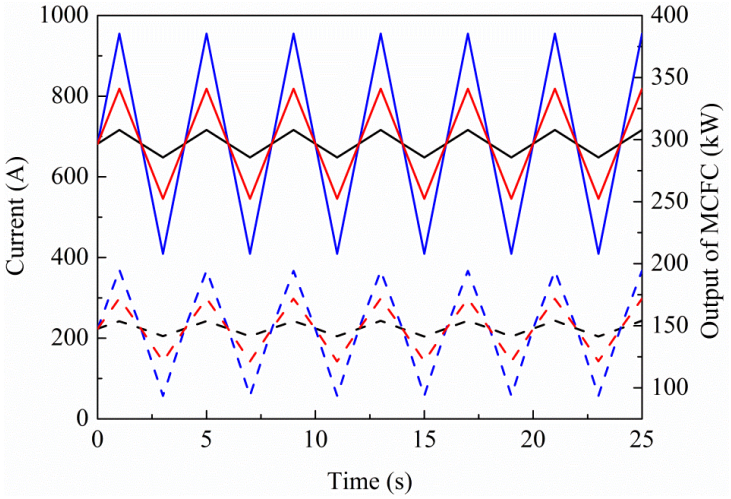

Figure 12. Output response of current (solid line) and output of MCFC (dashed line) at varied power demands changes of 5% (black), 20% (red), and 40% (blue) at current change speed of $\pi/2$.

4. Conclusions

The performance of an MCFC/MGT hybrid power system bi-fueled by city gas and biogas was evaluated in this study. The effects of biogas with added city gas as a bi-fuel for MCFC/MGT power and the MFCF/MGT hybrid power system response were investigated experimentally and numerically. The major conclusions in this study are as follows:

(1) The MCFC, steam reformer, and catalytic combustor models are in good agreement with the experimental results fueled by city gas only or bi-fueled by city gas and biogas.
(2) The MFCF/MGT hybrid power system can be operated stably with added biogas flow rate up to 150.0 $Nm^3 \cdot h^{-1}$, which is about 50% of the overall input heat value with high overall power generation efficiency ranging from 39.0% to 42.0%.
(3) The MCFC/MGT hybrid power system can be operated stably both at low amplitude with slow current change speeds and large amplitude with rapid power demand conditions.
(4) The MCFC/MGT hybrid system bi-fueled by city gas and biogas is applicable in providing energy for the micro–grid network with wide amplitude.

Author Contributions

Hongyu Huang performed the experimental measurements, analysis and simulations, and largely wrote this article. Jun Li, Zhaohong He and Tao Zeng contributed to MCFC experimental measurements and modeling process. Noriyuki Kobayashi and Mitsuhiro Kubota contributed to the analysis and the writing of this article.

Conflicts of Interest

The authors declare no conflict of interest.

Nomenclature

A	heat transfer area (m^2)
A_a	the frequency factor of anode ($ohm \cdot cm^2 \cdot atm^{0.5} \cdot k^{-1}$)
A_c	the frequency factor of cathode ($ohm \cdot cm^2 \cdot atm^{0.5} \cdot k^{-1}$)
A_{ir}	the frequency factor of internal resistance on electrolyte ($ohm \cdot cm^2$)
cat_w	catalyst weight (kg)
$n(e^-)$	the mole flow of electrons ($kmol \cdot h^{-1}$)
E	Nernst voltage (V)
E^0	standard electrode potential (V)
F	Faraday constant ($s \cdot A \cdot mol^{-1}$)
F_{inlet}	inlet flow rate of gas ($kmol \cdot h^{-1}$)
F_{outlet}	outlet flow rate of gas ($kmol \cdot h^{-1}$)
h	heat transfer coefficient ($W \cdot m^{-2} \cdot K^{-1}$)
ΔH_a	activation energy of anode
ΔH_c	activation energy of cathode
ΔH_{ir}	activation energy of internal resistance of the electrolyte ($kJ \cdot mol^{-1}$)
i	current value (A)
j	current density ($A \cdot m^2$)
k	reaction rate constant
Nu	Nusselt number
P	pressure (atm)

Pr	Prandtl number
Q	reaction heat (J)
R_a	anode resistance (ohm·cm^2)
R_c	cathode resistance (ohm·cm^2)
R_{ir}	internal resistance on the electrolyte (ohm·cm^2)
Re	Reynolds number
r	reaction rate (kmol·h^{-1})
T	temperature (K)
U_f	fuel efficiency (-)

References

1. Raj, N.T.; Iniyan, S.; Goic, R. A review of renewable energy based cogeneration technologies. *Renew. Sustain. Energy Rev.* **2011**, *15*, 3640–3648.
2. Bocci, E.; Carlo, D.A.; Mcphail, S.J.; Gallucci, K.; Fosolo, P.U.; Moneti, M.; Villarini, M.; Carlini, M. Biomass to fuel cells state of the art: A review of the most innovative technology solutions. *Int. J. Hydrog. Energy* **2014**, *39*, 21876–21895.
3. Lorenzo, D.G.; Fragiacomo, P. A methodology for improving the performance of molten carbonate fuel cell/gas turbine hybrid systems. *Int. J. Energy Res.* **2012**, *36*, 96–110.
4. Chacartegui, R.; Blanco, M.J.; Muñoz-de-Escalona, J.M.; Sánchez, D.; Sánchez, T. Performance assessment of molten carbonate fuel cell-humid air turbine hybrid system. *Appl. Energy* **2013**, *102*, 687–699.
5. Molino, A.; Giordano, G.; Motola, V.; Fiorenza, G.; Nana, F.; Graccio, G. Electricity production by biomass steam gasification using a high efficiency technology and low environmental impact. *Fuel* **2013**, *103*, 179–192.
6. Vera, D.; Jurado, F.; Panopoulos, K.D.; Grammelis, P. Modelling of biomass gasifier and microturbine for the olive oil industry. *Int. J. Energy Res.* **2012**, *36*, 355–367.
7. Liu, A.G.; Wang, B.; Zeng, W.; Chen, B.D.; Weng, Y.W. Catalytic combustion and system performance assessment of MCFC-MGT hybrid system. *Int. J. Hydrog. Energy* **2014**, *39*, 7437–7446.
8. Campanari, S.; Manzolini, G.; Chiesa, P. Using MCFC for high efficiency CO_2 capture from natural gas combined cycles: Comparison of internal and external reforming. *Appl. Energy* **2013**, *112*, 772–783.
9. Chao, Y.C.; Chen, G.B.; Hsu, H.W.; Hsu, J.R. Catalytic combustion of gasified biomass in a platinum monolith honeycomb reactor. *Appl. Catal. A Gen.* **2004**, *261*, 99–107.
10. Verda, V.; Sciacovelli, A. Optimal design and operation of a biogas fuelled MCFC (molten carbonate fuel cells) system integrated with an anaerobic digester. *Energy* **2012**, *47*, 150–157.
11. Kawase, M.; Mugikura, Y.; Izaki, Y.; Watanabe, T.; Ito, Y. Effects of fluoride on the performance of MCFCs. *J. Power Sources* **2003**, *124*, 52–58.
12. Papurello, D.; Lazini, A.; Leone, P.; Santarelli, M.; Silvestri, S. Biogas from the organic fraction of municipal solid waste: Dealing with contaminants for a solid oxide fuel cell energy generator. *Waste Manag.* **2014**, *34*, 2047–2056.

13. Bedont, P.; Grillo, O.; Massardo, A.F. Off-design performance analysis of a hybrid system based on existing molten fuel cell stack. *J. Eng. Gas Turbines Power* **2003**, *125*, 986–993.
14. Lundberg, W.L.; Veyo, S.E.; Moeckel, M.D. A high-efficiency solid oxide fuel cell hybrid power system using the mercury 50 advanced turbine systems gas turbine. *J. Eng. Gas Turbines Power* **2003**, *125*, 51–58.
15. Galvagno, A.; Chiodo, V.; Urbani, F.; Freni, F. Biogas as hydrogen source for fuel cell applications. *Int. J. Hydrog. Energy* **2013**, *38*, 3913–3920.
16. Wee, J.H. Molten carbonate fuel cell and gas turbine hybrid systems as distributed energy resources. *Appl. Energy* **2011**, *88*, 4252–4263.
17. Liu, A.G.; Weng, Y.W. Performance analysis of a pressurized molten carbonate fuel cell/micro-gas turbine hybrid system. *J. Power Sources* **2010**, *195*, 204–213.
18. Lunghi, P.; Bove, R.; Desideri, U. Analysis and optimization of hybrid MCFC gas turbines plants. *J. Power Sources* **2003**, *118*, 108–117.
19. Kivisaari, T.; Björnbom, P.; Sylwan, C. Studies of biomass fueled MCFC systems. *J. Power Sources* **2002**, *104*, 115–124.
20. Hamad, T.A.; Agil, A.A.; Hamad, Y.M.; Bapat, S.; Thomas, M.; Martin, K.B.; Sheffield, J.M. Study of combined heat, hydrogen and power system based on a molten carbonate fuel cell fed by biogas produced by anaerobic digestion. *Energy Convers. Manag.* **2014**, *81*, 184–191.
21. Milewski, J.; Discepoli, G.; Desideri, U. Modeling the performance of MCFC for various fuel and oxidant compositions. *Int. J. Hydrog. Energy* **2014**, *39*, 11713–11721.
22. Bove, R.; Lunghi, P. Experimental comparison of MCFC performance using three different biogas types and methane. *J. Power Sources* **2005**, *145*, 588–593.
23. Freni, S.; Cavallaro, S. Catalytic partial oxidation of methane in a molten carbonate fuel cell. *Int. J. Hydrog. Energy* **1999**, *24*, 75–82.
24. Zanfir, M.; Gavriilidis, A. Catalytic combustion assisted methane steam reforming in a catalytic plate reactor. *Int. J. Hydrog. Energy* **2014**, *39*, 11713–11721.
25. Freni, S.; Aquino, M.; Giordano, N. Mass and energy balances in a molten-carbonate fuel cell with internal reforming. *J. Power Sources* **1992**, *39*, 203–214.
26. NIST-JANAF Thermochemical Tables. Available online: http://kinetics.nist.gov/janaf/ (accessed on 15 June 2014).